RESEARCH PAPER

CeO_2/CuO@N-GQDs@NH_2 nanocomposite as a reusable and efficient catalyst for the synthesis of piperidines

Hossein Shahbazi-Alavi[1*] Javad Safaei-Ghomi[2] Mozhgan Esfandiari[3]

[1] Young Researchers and Elite Club, Kashan Branch, Islamic Azad University, Kashan, Iran

[2] Department of Organic Chemistry, Faculty of Chemistry, University of Kashan, Kashan, Iran

[3] Department of Chemistry, Shiraz Branch, Islamic Azad University, Shiraz, Iran

ARTICLE INFO

Article History:
Received 11 November 2019
Accepted 08 January 2020
Published 15 February 2020

Keywords:
Graphene Quantum Dots
Nanocomposite
Nanocatalyst
Piperidines

ABSTRACT

An efficient pseudo six-component synthesis of bis-spiropiperidines is presented by one-pot condensation of formaldehyde, aromatic amine and dimedone or N,N-dimethyl-barbituric acid using CeO_2/CuO@N-GQDs@NH_2 nanocomposite at room temperature. The catalyst has been characterized by SEM, FT-IR, XRD, EDS, TGA, BET, VSM and XPS. Atom economy, reusable catalyst, low catalyst loading, applicability to a wide range of substrates and high yields of products are some of the notable features of this method.

How to cite this article
Shahbazi-Alavi H, Safaei-Ghomi J, Esfandiari M. CeO_2/CuO@N-GQDs@NH_2 nanocomposite as a reusable and efficient catalyst for the synthesis of piperidines. Nanochem Res, 2020; 5(1):25-34. DOI: 10.22036/ncr.2020.01.003

INTRODUCTION

Piperidines indicate antibacterial [1], antihistaminic [2], anticonvulsants [3], anti-AIDS [4], anticancer [5] inhibitor [6] and anti-virus activities [7]. Piperidines have been regarded as notable targets of organic synthesis. Therefore, searching for effective ways for the preparation of piperidines is a notable challenge. A number of methods have been improved for the synthesis of piperidines in the presence of catalysts such as iron(III) chloride [8], tartaric acid [9], $ZrCl_4$ [10], CH_3COOH [11,12] silica supported tungstic acid (STA) [13], iron(III) trifluroacetate [14], cerium supported on chitosan [15], Dy (III)/chitosan [16], and silica-supported copper [17]. Some of the reported methods endure drawbacks such as long reaction times, use of toxic and non-reusable catalyst and undesirable reaction conditions. Hence, to avoid these disadvantages, the finding of an effective procedure for the preparation of piperidines is still favored.

Metal oxides indicate a broad class of materials that have been researched extensively owing to their unique attributes and potential usages in various fields [18]. N-GQDs have gained intensive regard owing to the significant features containing stabilizing the antibodies [19], biological [20], drug delivery [21], photocatalysts [22], surfactants [23], bioelectronics [24], electrocatalytic [25], Li-ion battery [26], solar cells [27], photoluminescence [28,29], bioimaging properties [30], and catalytic activity [31]. Potential applications of N-graphene quantum dots were newly reviewed on the basis of theoretical and experimental studies [32-35]. Herein, we reported the use of CeO_2/CuO@N-GQDs@NH_2 nanocomposite as an efficient catalyst for the preparation of bis-spiropiperidines by one-pot condensation of formaldehyde, aromatic amine and dimedone or N,N-dimethyl-barbituric acid at room temperature (Scheme 1).

* Corresponding Author Email: *hossien_shahbazi@yahoo.com*

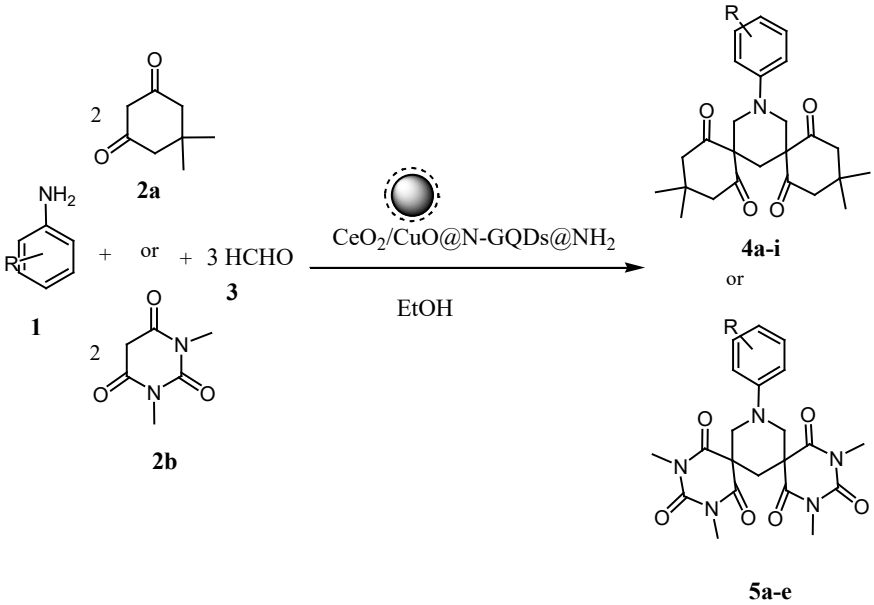

Scheme 1. Synthesis of bis-spiropiperidines using the CeO_2/CuO@N-GQDs@NH_2 nanocomposite

EXPERIMENTAL SECTION

Preparation of CeO_2/CuO nanoparticles:

($Ce(SO_4)_2.4H_2O$) and $CuCl_2.2H_2O$ with 1:1 molar ratio were dissolved in deionized water. Afterward, an appropriate amount of aqueous sodium hydroxide solution (0.70 M) was added to the above solution until the pH value reached 10. Then, transparent solution was placed in autoclave at 120 °C for 6 h. The obtained precipitate was washed twice with methanol and dried at 60 °C for 5h. Finally, the product was calcined at 500 °C for 2h.

Preparation of CeO_2/CuO @N-GQDs nanocomposite: 1 g citric acid was dissolved into 20 mL deionized water, and stirred to form a clear solution. After that, 0.3 mL ethylenediamine was added to the above solution and mixed to obtain a clear solution. Then, 0.1 g CeO_2/CuO nanoparticles was added to the mixture. The mixture was stirred at room temperature within 5 minutes. Then, the solution was transferred into a 50 mL Teflon lined stainless autoclave. The sealed autoclave was heated to 180°C for 9 h in an electric oven. Finally, as-prepared nanostructured CeO_2/CuO @N- GQDs was obtained, washed several times with deionized water and ethanol, and then dried in an oven until constant weight was achieved.

Preparation of CeO_2/CuO@N-GQDs@NH_2 nancomposite: 1g of CeO_2/CuO@N-GQDs nanocomposite was added to the solution of 3-aminopropyltriethoxysilane (2 mmol, 0.44 g) in dry toluene (20 mL) and refluxed for 24 h. After completing the reaction, the aminated- CeO_2/CuO@N-GQDs were separated by a centrifuge, washed with double-distilled water and anhydrous ethanol, and dried at 80 °C for 8 h to give the surface bound amino group CeO_2/CuO@N-GQDs@NH_2.

General procedure for the preparation of bisspiropiperidines:

A mixture of formaldehyde (3 mmol), dimedone or N,N-dimethyl-barbituric (2 mmol) aniline derivatives (1 mmol) and CeO_2/CuO@N-GQDs@NH_2 nanocomposites (4 mg) in ethanol (10 mL) was stirred at room temperature. The reaction was monitored by TLC. After completion of the reaction, the catalyst was insoluble in ethyl acetate and it could therefore be recycled by a simple filtration. Water was added, and the precipitate was collected by filtration and washed with water. The crude product was recrystallized or washed with ethanol to give the pure product.

15-(4-Chloro phenyl)-3,3,11,11-tetramethyl-15-azadispiro [5.1.5.3]hexadecane-1,5,9,13-tetrone (4a): White solid, mp 216–218 °C. IR (KBr, ν_{max} /cm^{-1}): 2963, 2925, 2864, 2832, 2796, 1727, 1736, 1705, 1694, 1595, 1496, 1432, 1342, 1248, 824, 674, 515. ^{1}H NMR (400 MHz, $CDCl_3$): δ 1.04 (s, 12H, CH_3), 2.52 (s, 2H, CH_2), 2.64 (d, J = 12.0 Hz, 4H,

$COCH_2$), 2.85 (d, *J* = 12.0 Hz, 4H, $COCH_2$), 3.44 (s, 4H, NCH_2), 7.05 (d, *J* = 8.4 Hz, 2H, Ar–H), 7.26 (d, *J* = 8.4 Hz, 2H, Ar–H) ppm. ^{13}C NMR (100 MHz, $CDCl_3$): δ 28.5, 28.6, 30.8, 32.3, 51.3, 54.9, 65.6, 120.2, 126.4, 129.1, 150.3, 205.9 ppm. Anal. Calcd for $C_{25}H_{30}ClNO_4$: C, 67.63; H, 6.81; N, 3.15. Found: C, 67.72; H, 6.85; N, 3.24.

15-(4-Bromo phenyl)-3,3,11,11-tetramethyl-15-azadispiro [5.1.5.3]hexadecane-1,5,9,13-tetrone (4b): Yellow solid, mp 200–202 °C. IR (KBr, ν_{max} / cm^{-1}): 2952, 1732, 1724, 1706, 1692, 1586, 1493, 1245, 1223, 1146, 1075, 824, 662, 510. ^{1}H NMR (400 MHz, $CDCl_3$): δ 1.05 (s, 6H, CH_3), 1.06 (s, 6H, CH_3), 2.53 (s, 2H, CH_2), 2.68 (d, *J* = 13.6 Hz, 4H, $COCH_2$), 2.85 (d, *J* = 13.6 Hz, 4H, $COCH_2$), 3.46 (s, 4H, NCH_2), 7.02 (d, *J* = 7.2 Hz, 2H, Ar–H), 7.34 (d, *J* = 7.2 Hz, 2H, Ar–H) ppm. ^{13}C NMR (100 MHz, $CDCl_3$): δ 28.4, 28.5, 30.6, 32.3, 51.4, 54.7, 65.5, 120.6, 127.3, 128.3, 151.6, 205.7 ppm. Anal. Calcd for $C_{25}H_{30}BrNO_4$: C, 61.48; H, 6.19; N, 2.87; Found: C, 61.38; H, 6.12; N, 2.76.

15-(4-Nitro phenyl)-3,3,11,11-tetramethyl-15-azadispiro [5.1.5.3] hexadecane-1,5,9,13-tetrone (4c): Yellow solid, mp 224–226 °C. IR (KBr, ν_{max} / cm^{-1}): 2954, 2932, 2873, 1727, 1703, 1594, 1496, 1327, 1225, 664, 503. ^{1}H NMR (400 MHz, DMSO): δ 0.98 (s, 6H, CH_3), 1.02 (s, 6H, CH_3), 2.63 (s, 2H, CH_2), 2.75 (d, *J* = 12.0 Hz, 4H, $COCH_2$), 2.87 (d, *J* = 12.0 Hz, 4H, $COCH_2$), 3.85 (s, 4H, NCH_2), 7.25 (d, *J* = 8.6 Hz, 2H, Ar–H), 8.07 (d, *J* = 8.6 Hz, 2H, Ar–H) ppm. ^{13}C NMR (100 MHz, DMSO): δ 27.8, 28.2, 31.2, 32.5, 49.3, 50.6, 64.8, 117.7, 125.9, 135.1, 153.7, 206.9 ppm. Anal. Calcd for $C_{25}H_{30}N_2O_6$: C, 66.06; H, 6.65; N, 6.16. Found: C, 66.15; H, 6.78; N, 6.24.

15-(3-Nitro phenyl)-3,3,11,11-tetramethyl-15 azadispiro [5.1.5.3]hexadecane-1,5,9,13-tetrone (4d): Yellow solid, mp 187–189 °C. IR (KBr, ν_{max} /cm^{-1}): 2954, 2929, 1725, 1706, 1537, 1342, 1203, 873, 786, 678. ^{1}H NMR (400 MHz, $CDCl_3$): δ 1.02 (s, 6H, CH_3), 1.04 (s, 6H, CH_3), 2.56 (s, 2H, CH_2), 2.67 (d, *J* = 12.0 Hz, 4H, $COCH_2$), 2.89 (d, *J* = 12.0 Hz, 4H, $COCH_2$), 3.56 (s, 4H, NCH_2), 7.43-7.76 (m, 4H, Ar–H) ppm. ^{13}C NMR (100 MHz, $CDCl_3$): δ 28.4, 28.6, 30.7, 32.5, 51.4, 53.5, 65.6, 112.9, 115.6, 124.8, 129.7, 149.2, 151.6, 205.6 ppm. Anal. Calcd for $C_{25}H_{30}N_2O_6$: C, 66.06; H, 6.65; N, 6.16. Found: C, 66.14; H, 6.75; N, 6.24.

15-(2,3-Dichloro phenyl)-3,3,11,11-tetramethyl-15-azadispiro [5.1.5.3]hexadecane-1,5,9,13-tetrone (4e): White solid, mp 250–252 °C. IR (KBr, ν_{max} / cm^{-1}): 2965, 2938, 2932, 1726, 1705, 1693, 1585, 1476, 1256, 1223, 990, 765, 668. ^{1}H NMR (400 MHz, $CDCl_3$): δ 1.04 (s, 12H, CH_3), 2.52 (s, 2H, CH_2), 2.67 (d, *J* = 14.0 Hz, 4H, $COCH_2$), 2.86 (d, *J* = 14.0 Hz, 4H, $COCH_2$), 3.45 (s, 4H, NCH_2), 7.03 (d, *J* = 8.2 Hz, 1H, Ar–H), 7.16 (t, *J* = 8.0 Hz, 1H, Ar–H), 7.39 (d, *J* = 8.8 Hz, 1H, Ar–H) ppm. ^{13}C NMR (100 MHz, $CDCl_3$): δ 28.3, 28.6, 30.7, 32.3, 51.3, 54.5, 65.5, 118.7, 119.8, 124.6, 130.5, 132.9, 150.7, 205.9 ppm. Anal. Calcd for $C_{25}H_{29}Cl_2NO_4$: C, 62.76; H, 6.11; N, 2.93. Found: C, 62.63; H, 6.22; N, 2.86.

15-(4-methyl phenyl)-3,3,11,11-tetramethyl-15-azadispiro [5.1.5.3]hexadecane-1,5,9,13-tetrone (4f): White solid, mp: 198–200 °C; IR (KBr, ν_{max} / cm^{-1}): 2950, 2932, 1721, 1706, 1536, 1343, 677; ^{1}H NMR (400 MHz, $CDCl_3$) δ 1.04 (12H, s, CH_3), 2.05 (3H, s, CH_3), 2.44 (2H, s, CH_2), 2.69 (4H, d, *J* = 13.8 Hz, $COCH_2$), 2.87 (4H, d, *J* = 13.8 Hz, $COCH_2$), 3.52 (4H, s, NCH_2), 7.28 (2H, d, *J* = 8.0 Hz, ArH), 7.49 (2H, d, *J* = 8.0 Hz, ArH); ^{13}C NMR (100 MHz, $CDCl_3$): δ 20.7, 28.5, 28.6, 30.9, 32.3, 51.6, 55.8, 66.2,119.6, 129.2, 131.8, 149.5, 206.8 ppm; Anal. Calcd for $C_{26}H_{33}NO_4$: C, 73.73; H, 7.85; N, 3.31. Found: C, 73.79; H, 7.94; N, 3.25.

RESULTS AND DISCUSSION

We prepared CeO_2/CuO nanoparticles by easy techniques. A hydrothermal way was used for the preparation of N-GQDs [36]. Amino-functionalized graphene quantum dots were prepared using 3-aminopropyltriethoxysilane. XRD pattern of CeO_2/CuO, and CeO_2/CuO@N-GQDs@NH_2 nanocomposite is shown in Fig. 1. The XRD pattern confirms the presence of both CuO (JCPDS No.89-2529) and CeO_2 (JCPDS No 34-0394).

In order to consider the particle size and morphology of the nanocatalyst, the SEM images of CeO_2/CuO and CeO_2/CuO@N-GQDs@NH_2 nanocomposite were provided; Fig. 2. The SEM images of the CeO_2/CuO@N-GQDs@NH_2 nanocomposite showed the formation of uniform particles, and the energy-dispersive X-ray spectrum (EDS) confirmed the presence of Ce, Cu, O, N and C species in the structure of the nanocomposite (Fig. 3).

Magnetic properties of nanocomposites before

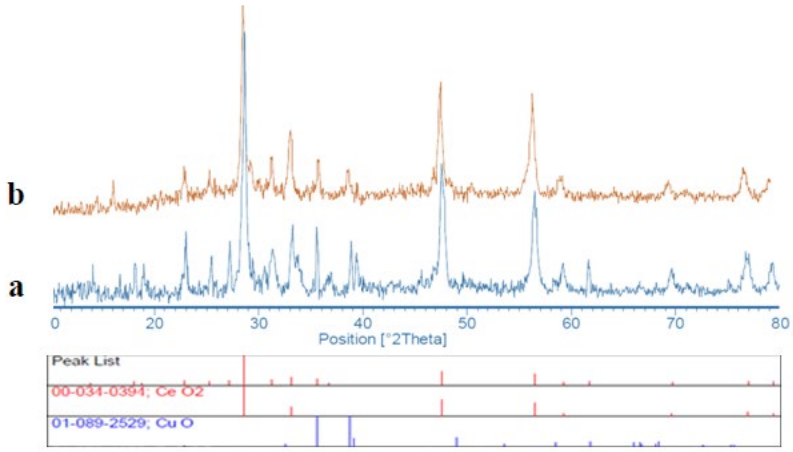

Fig. 1. XRD pattern of (a) CeO_2/CuO, and (b) CeO_2/CuO@N-GQDs@NH_2

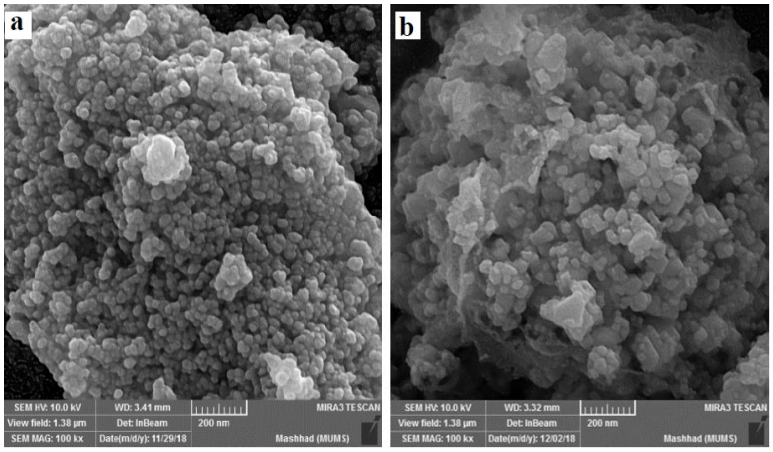

Fig. 2. SEM images of (a) CeO_2/CuO, and (b) CeO_2/CuO@N-GQDs@NH_2

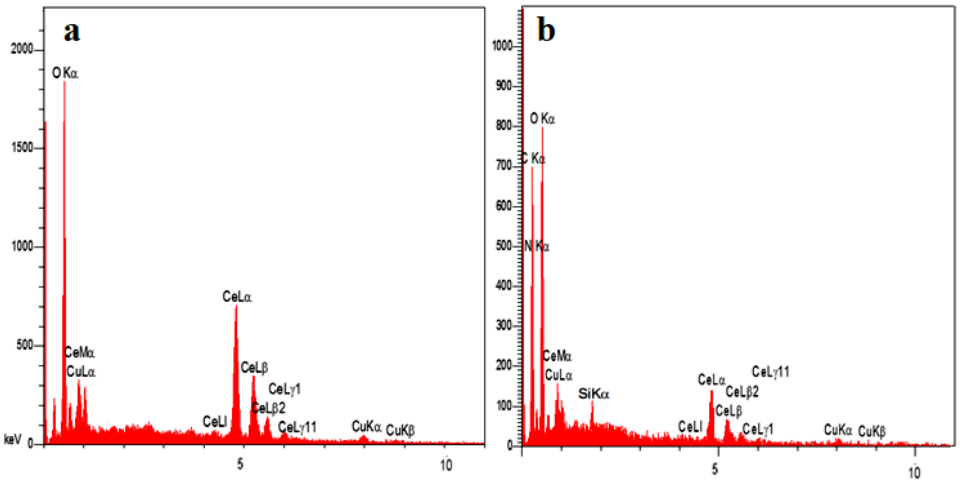

Fig. 3. EDS spectra of (a) CeO_2/CuO, and (b) CeO_2/CuO@N-GQDs@NH_2

and after their being decorated with N-GQDs were tested by vibrating-sample magnetometer (VSM) (Fig. 4). The lower magnetism of the as-synthesized CeO_2/CuO@N-GQDs@NH_2 compared to the CeO_2/CuO nanocomposite was ascribed to the antiferromagnetic behavior of N-GQDs as a dopant.

FT-IR spectra of CeO_2/CuO, CeO_2/CuO@N-GQDs and CeO_2/CuO@N-GQDs@NH_2 nanocomposite are indicated in Fig. 5. The absorption peak at 3300 cm^{-1} is related to the stretching vibrational absorptions of OH. The peaks at 509, 663cm^{-1} corresponded to Cu-O and Ce-O, respectively. The characteristic peaks at 3400 cm^{-1} (O-H stretching vibration), 1660 cm^{-1} (C=O stretching vibration), and 1101 cm^{-1} (C-O-C stretching vibration) appear in the spectrum of Figure 5b. The peak at approximately 1475-1580 cm^{-1} is attributed to C=C bonds. The peaks at 1560 and 3350 cm^{-1} are related to the bending and stretching vibrational absorptions of N-H, respectively (Fig 5c).

The BET specific surface area of CeO_2/CuO and CeO_2/CuO@N-GQDs@NH_2 nanocomposites was measured by the nitrogen gas adsorption-desorption isotherms (Fig. 6). Based on the results, the BET specific surface area of CeO_2/CuO was improved from 1.72 to 9.82 m^2/g after modification with N-GQDs, therefore, more active sites were introduced on CeO_2/CuO@N-GQDs@NH_2 surface.

Thermogravimetric analysis (TGA) considers

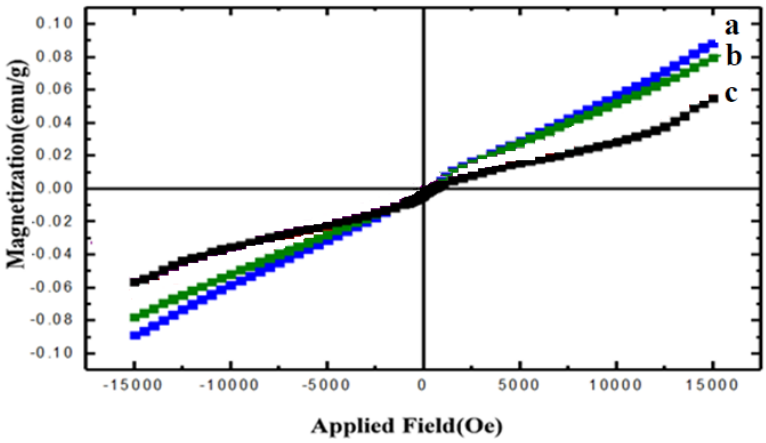

Fig. 4. VSM of (a) CeO_2/CuO, (b) CeO_2/CuO@N-GQDs, and (c) CeO_2/CuO@N-GQDs@NH_2

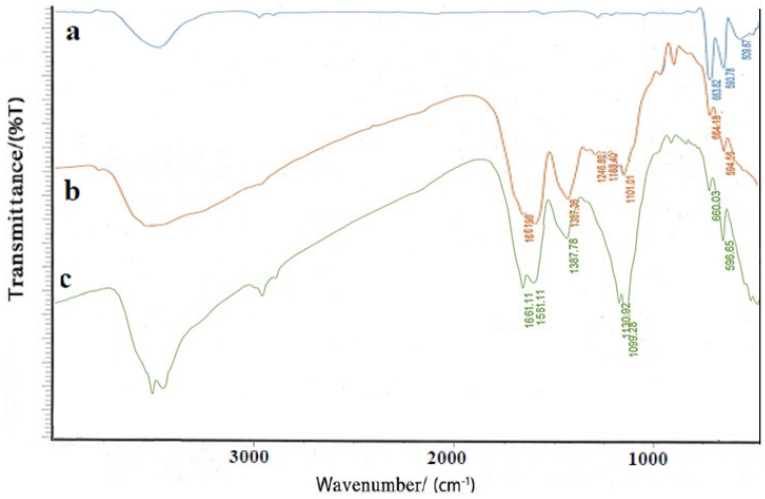

Fig. 5. FT-IR of (a) CeO_2/CuO, (b) CeO_2/CuO@N-GQDs, and (c) CeO_2/CuO@N-GQDs@NH_2

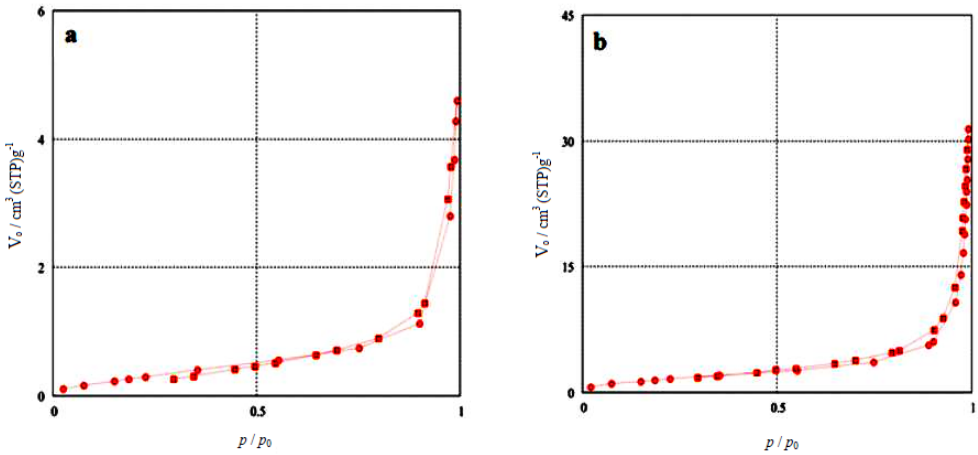

Fig. 6. The BET specific surface area of (a) CeO_2/CuO, and (b) CeO_2/CuO@N-GQDs@NH_2

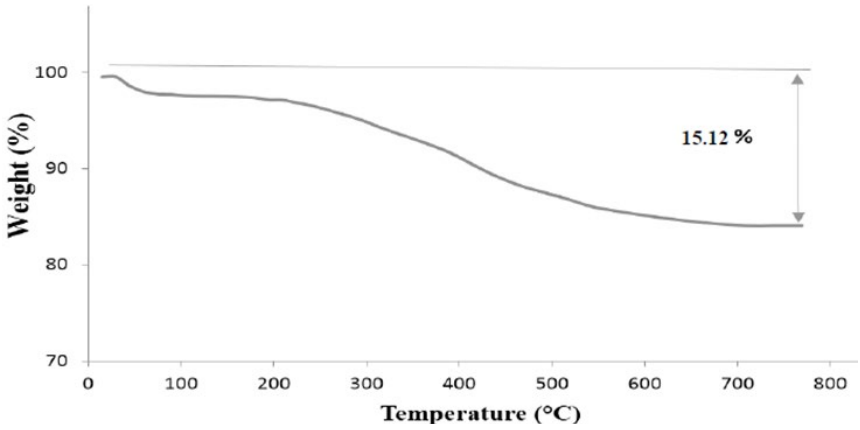

Fig. 7. TGA of CeO_2/CuO@N-GQDs@NH_2

the thermal stability of the CeO_2/CuO@N-GQDs@NH_2 nanocomposites (Fig. 7). These nanoparticles show suitable thermal stability without a significant decrease in weight. The weight loss (2.14%) at temperatures below 200 °C is due to the removal of physically adsorbed solvent and surface hydroxyl groups. The curve displays a weight loss about 12.98% from 200 to 600 °C that is attributed to the oxidation, degradation of N-GQD and decomposition of the organic spacer grafting to the N-GQD surface.

X-ray photoelectron spectroscopy (XPS) analysis of CeO_2/CuO@N-GQDs@NH_2 nanocomposite is shown in Figure 8. In the wide-scan spectrum of nanocatalyst, the predominant components are Cu 2p (940-970 eV), Ce 3d (883.8 eV), O 1s (530.6 eV), N 1s (400 eV), and C 1s (286.3 eV).

At first, we investigated three-component reaction of formaldehyde, 4-methylaniline and dimedone as a model reaction. The model reactions were performed by *p*TSA, $BF_3.SiO_2$, $ZrOCl_2$, Et_3N, CeO_2/CuO, CeO_2/CuO@N-GQDs and CeO_2/CuO@N-GQDs@NH_2 nanocomposite. The best results were gained in EtOH and we found the convincing results in the presence of CeO_2/CuO@N-GQDs@NH_2 nanocomposite (4 mg) at room temperature (Table 1).

To investigate the scope and limitation of this catalytic process, formaldehyde, aromatic amines and dimedone or N, N-dimethyl-barbituric acid were chosen as substrates (Table 2). Investigations of the reaction scope revealed that various aromatic amines (bearing electron-withdrawing and electron-donating groups) can be utilized in this protocol.

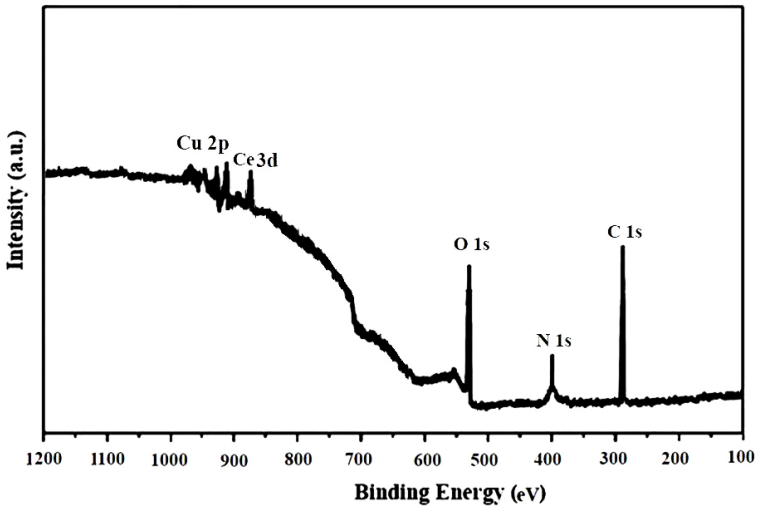

Fig. 8. X-ray photoelectron spectroscopy (XPS) analysis of CeO_2/CuO@N-GQDs@NH_2 nanocomposite

Table 1. Optimization of the reaction conditions using different catalysts [a]

Entry	Catalyst (amount)	Solvent	Time (min)	Yield[a] %
1	none	EtOH	400	NR
2	*p*TSA (4 mol%)	EtOH	400	12
3	$BF_3.SiO_2$ (8 mol%)	EtOH	350	29
4	$ZrOCl_2$ (5 mol%)	EtOH	300	39
5	Et_3N (5 mol%)	EtOH	400	58
6	CeO_2/CuO nanocomposite	EtOH	250	52
7	CeO_2/CuO@N-GQDs nanocomposite	EtOH	150	74
8	CeO_2/CuO@N-GQDs@NH_2 nanocomposite (3 mg)	EtOH	60	88
9	CeO_2/CuO@N-GQDs@NH_2 nanocomposite (4 mg)	EtOH	60	93
10	CeO_2/CuO@N-GQDs@NH_2 nanocomposite (5 mg)	EtOH	60	93
11	CeO_2/CuO@N-GQDs@NH_2 nanocomposite (4 mg)	H_2O	150	72
12	CeO_2/CuO@N-GQDs@NH_2 nanocomposite (4 mg)	DMF	120	77
13	CeO_2/CuO@N-GQDs@NH_2 nanocomposite (4 mg)	CH_3CN	95	82

[a] Formaldehyde (3 mmol), 4-methylaniline (1 mmol) and dimedone (2 mmol)
[b]Isolated yield

Table 2. Synthesis of bis-spiropiperidines using CeO_2/CuO@N-GQDs@NH_2 [a]

Entry	R	di carbonyl compound	Product	Time (min)	Yield[a]%	m.p °C (Found)	m.p °C [ref]
1	4-Cl	dimedone	4a	60	88	216-218	216-218 [12]
2	4-Br	dimedone	4b	120	88	200-202	200-202 [14]
3	4-NO_2	dimedone	4c	120	83	224-226	220-222 [14]
4	3-NO_2	dimedone	4d	120	85	187-189	187-189 [12]
5	2,3-dichloro	dimedone	4e	120	85	250-252	—
6	4-CH_3	dimedone	4f	120	93	198-200	199-201 [15]
7	4-NO_2	N,N-dimethyl-barbituric acid	5a	140	80	270-272	—
8	4-Cl	N,N-dimethyl-barbituric acid	5b	140	82	230-232	—
9	2-NO_2	N,N-dimethyl-barbituric acid	5c	145	81	261-263	—
10	4-Br	N,N-dimethyl-barbituric acid	5d	140	83	215-217	—
11	4-CH_3	N,N-dimethyl-barbituric acid	5e	140	90	247-249	—

[a] Isolated yield

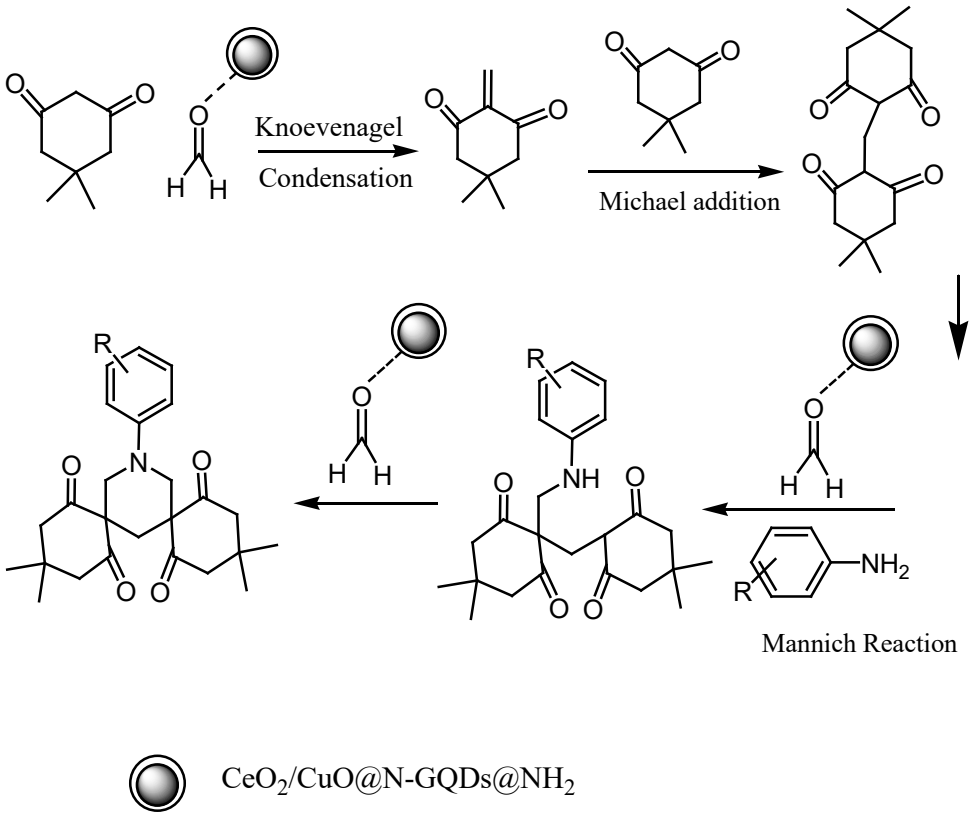

Scheme 2. Possible mechanism of the one-pot reaction for the preparation of bis-spiropiperidines

The reusability of the CeO_2/CuO@N-GQDs@NH_2 nanocomposite catalyst was examined for the model reaction and it was found that the product yields decreased to a small extent on each reuse (run 1, 93%; run 2, 93%; run 3, 92%; run 4, 92%; run 5, 91%, run 6, 91%).

A plausible mechanism for the preparation of bis-spiropiperidines is shown in Scheme 2. The spirocyclization looks to proceed as a domino sequence of Knoevenagel, Michael, and double Mannich reactions. The well-known reaction of dimedone with formaldehyde leads to the formation of the standard dimedone–formaldehyde adducts. In cycle, this undergoes two consecutive Mannich reactions with aniline to produce the spiro-piperidine. The amino groups distributed on the surface of CeO_2/CuO@N-GQDs activate the C=O and C≡N groups through hydrogen bonding [37-40].

CONCLUSION

We have reported an efficient method for the synthesis of bis-spiropiperidines using CeO_2/CuO@N-GQDs@NH_2 nanocomposite as a superior catalyst at room temperature. The new catalyst is characterized by SEM, FT-IR XRD, EDS, TGA, BET, VSM and XPS. The current method provides obvious positive points containing environmental friendliness, reusability of the catalyst, low catalyst loading and simple experimental.

ACKNOWLEDGEMENT

The authors are grateful to University of Kashan for supporting this work by Grant NO: 159196/XXX.

CONFLICT OF INTEREST

The authors confirm that this article content has no conflict of interest.

REFERENCES

1. Zhou Y, Gregor VE, Ayida BK, Winters GC, Sun Z, Murphy D, et al. Synthesis and SAR of 3,5-diamino-piperidine derivatives: Novel antibacterial translation inhibitors as aminoglycoside mimetics. Bioorganic & Medicinal Chemistry Letters. 2007;17(5):1206-10.
2. Weis R, Schweiger K, Faist J, Rajkovic E, Kungl AJ, Fabian WMF, et al. Antimycobacterial and H1-antihistaminic activity of 2-substituted piperidine derivatives. Bioorganic

& Medicinal Chemistry. 2008;16(24):10326-31.
3. Ho B, Michael Crider A, Stables JP. Synthesis and structure–activity relationships of potential anticonvulsants based on 2-piperidinecarboxylic acid and related pharmacophores. European Journal of Medicinal Chemistry. 2001;36(3):265-86.
4. Finke PE, Meurer LC, Oates B, Shah SK, Loebach JL, Mills SG, et al. Antagonists of the human CCR5 receptor as anti-HIV-1 agents. Part 3: A proposed pharmacophore model for 1-[N-(methyl)-N-(phenylsulfonyl)amino]-2-(phenyl)-4-[4-(substituted)piperidin-1-yl]butanes. Bioorganic & Medicinal Chemistry Letters. 2001;11(18):2469-73.
5. Li J, Wu N, Tian Y, Zhang J, Wu S. Aminopyridyl/Pyrazinyl Spiro[indoline-3,4′-piperidine]-2-ones As Highly Selective and Efficacious c-Met/ALK Inhibitors. ACS Medicinal Chemistry Letters. 2013;4(8):806-10.
6. Kamata M, Yamashita T, Kina A, Funata M, Mizukami A, Sasaki M, et al. Design, synthesis, and structure–activity relationships of novel spiro-piperidines as acetyl-CoA carboxylase inhibitors. Bioorganic & Medicinal Chemistry Letters. 2012;22(11):3643-7.
7. Wang J, Cady SD, Balannik V, Pinto LH, DeGrado WF, Hong M. Discovery of Spiro-Piperidine Inhibitors and Their Modulation of the Dynamics of the M2 Proton Channel from Influenza A Virus. Journal of the American Chemical Society. 2009;131(23):8066-76.
8. Mukhopadhyay C, Rana S, Butcher RJ. FeCl3 catalysed two consecutive aminomethylation at the α-position of the β-dicarbonyl compounds: an easy access to hexahydropyrimidines and its spiro analogues. Tetrahedron Letters. 2011;52(32):4153-7.
9. Aboonajmi J, Maghsoodlou MT, Hazeri N, Lashkari M, Kangani M. Tartaric acid: a natural, green and highly efficient catalyst for the one-pot synthesis of functionalized piperidines. Research on Chemical Intermediates. 2014;41(11):8057-65.
10. Aboonajmi J, Mousavi MR, Maghsoodlou MT, Hazeri N, Masoumnia A. ZrCl4 as an efficient catalyst for one-pot synthesis of highly functionalized piperidines via multi-component organic reactions. Research on Chemical Intermediates. 2013;41(4):1925-34.
11. Lashkari M, Maghsoodlou MT, Hazeri N, Habibi-Khorassani SM, Sajadikhah SS, Doostmohamadi R. Synthesis of Highly Functionalized Piperidines via One-Pot, Five-Component Reactions in the Presence of Acetic Acid Solvent. Synthetic Communications. 2012;43(5):635-44.
12. Mousavi MR, Gharari H, Maghsoodlou MT, Hazeri N. Acetic acid-promoted eco-friendly one-pot pseudo six-component synthesis of bis-spiro-substituted piperidines. Research on Chemical Intermediates. 2015;42(4):3875-86.
13. Atar AB, Jeong YT. Silica supported tungstic acid (STA): an efficient catalyst for the synthesis of bis-spiro piperidine derivatives under milder condition. Tetrahedron Letters. 2013;54(10):1302-6.
14. Lohar T, Jadhav S, Kumbhar A, Mane A, Salunkhe R. Bis-amino methylation for the synthesis of spiro-fused piperidines using iron(III) trifluroacetate in aqueous micellar medium. Research on Chemical Intermediates. 2015;42(6):5329-38.
15. Ahmed N, Siddiqui ZN. Cerium Supported Chitosan as an Efficient and Recyclable Heterogeneous Catalyst for Sustainable Synthesis of Spiropiperidine Derivatives. ACS Sustainable Chemistry & Engineering. 2015;3(8):1701-7.
16. Ahmed N, Tarannum S, Siddiqui ZN. Dy/chitosan: a highly efficient and recyclable heterogeneous nano catalyst for the synthesis of hexahydropyrimidines in aqueous media. RSC Advances. 2015;5(63):50691-700.
17. Ray S, Bhaumik A, Banerjee B, Manna P, Mukhopadhyay C. Heterogeneous silica-supported copper catalyst for the ultrasound-mediated rapid reaction between dimedone, formaldehyde, and amines at room temperature. Monatshefte für Chemie - Chemical Monthly. 2015;146(11):1881-90.
[18] Shahbazi-Alavi H, Safaei-Ghomi J. Nano-colloidal silica-tethered polyhedral oligomeric silsesquioxanes with eight branches of 3-aminopropyltriethoxysilane as high performance catalyst for the preparation of furan-2(5H)-ones. Nanochemistry Research. 2019;4(1):11-9.
[19] Roushani M, Valipour A, Bahrami M. The potentiality of graphene quantum dots functionalized by nitrogen and thiol-doped (GQDs-NS) to stabilize the antibodies in designing of human chorionic gonadotropin immunosensor. Nano Chem Res. 2019;4:20-6.
20. Şenel B, Demir N, Büyükköroğlu G, Yıldız M. Graphene quantum dots: Synthesis, characterization, cell viability, genotoxicity for biomedical applications. Saudi Pharmaceutical Journal. 2019;27(6):846-58.
21. Molaei MJ. Carbon quantum dots and their biomedical and therapeutic applications: a review. RSC Advances. 2019;9(12):6460-81.
22. Yeh T-F, Teng C-Y, Chen S-J, Teng H. Nitrogen-Doped Graphene Oxide Quantum Dots as Photocatalysts for Overall Water-Splitting under Visible Light Illumination. Advanced Materials. 2014;26(20):3297-303.
23. Xi F, Zhao J, Shen C, He J, Chen J, Yan Y, et al. Amphiphilic graphene quantum dots as a new class of surfactants. Carbon. 2019;153:127-35.
24. Wang Y, Shao Y, Matson DW, Li J, Lin Y. Nitrogen-Doped Graphene and Its Application in Electrochemical Biosensing. ACS Nano. 2010;4(4):1790-8.
25. Li Q, Zhang S, Dai L, Li L-s. Nitrogen-Doped Colloidal Graphene Quantum Dots and Their Size-Dependent Electrocatalytic Activity for the Oxygen Reduction Reaction. Journal of the American Chemical Society. 2012;134(46):18932-5.
26. Reddy AL, Srivastava A, Gowda SR, Gullapalli H, Dubey M, Ajayan PM. Synthesis of Nitrogen-Doped Graphene Films for Lithium Battery Application. Defense Technical Information Center, 2010 2010/01/01. Report No.
27. Hasan MT, Gonzalez-Rodriguez R, Ryan C, Pota K, Green K, Coffer JL, et al. Nitrogen-doped graphene quantum dots: Optical properties modification and photovoltaic applications. Nano Research. 2019;12(5):1041-7.
28. Temerov F, Belyaev A, Ankudze B, Pakkanen TT. Preparation and photoluminescence properties of graphene quantum dots by decomposition of graphene-encapsulated metal nanoparticles derived from Kraft lignin and transition metal salts. Journal of Luminescence. 2019;206:403-11.
29. Zhu S, Shao J, Song Y, Zhao X, Du J, Wang L, et al. Investigating the surface state of graphene quantum dots. Nanoscale. 2015;7(17):7927-33.
30. Qu D, Zheng M, Li J, Xie Z, Sun Z. Tailoring color emissions from N-doped graphene quantum dots for bioimaging applications. Light: Science & Applications. 2015;4(12):e364-e.

31. Sajjadi S, Khataee A, Darvishi Cheshmeh Soltani R, Hasanzadeh A. N, S co-doped graphene quantum dot–decorated Fe3O4 nanostructures: Preparation, characterization and catalytic activity. Journal of Physics and Chemistry of Solids. 2019;127:140-50.
32. Du Y, Guo S. Chemically doped fluorescent carbon and graphene quantum dots for bioimaging, sensor, catalytic and photoelectronic applications. Nanoscale. 2016;8(5):2532-43.
33. Yan Y, Gong J, Chen J, Zeng Z, Huang W, Pu K, et al. Recent Advances on Graphene Quantum Dots: From Chemistry and Physics to Applications. Advanced Materials. 2019;31(21):1808283.
34. Li M, Chen T, Gooding JJ, Liu J. Review of Carbon and Graphene Quantum Dots for Sensing. ACS Sensors. 2019;4(7):1732-48.
35. Wang Z, Zeng H, Sun L. Graphene quantum dots: versatile photoluminescence for energy, biomedical, and environmental applications. Journal of Materials Chemistry C. 2015;3(6):1157-65.
36. Qu D, Zheng M, Du P, Zhou Y, Zhang L, Li D, et al. Highly luminescent S, N co-doped graphene quantum dots with broad visible absorption bands for visible light photocatalysts. Nanoscale. 2013;5(24):12272.
37. Safaei-Ghomi J, Shahbazi-Alavi H. Synthesis of dihydrofurans using nano-CuFe2O4@Chitosan. Journal of Saudi Chemical Society. 2017;21(6):698-707.
38. Safaei-Ghomi J, Shahbazi-Alavi H, Babaei P, Basharnavaz H, Pyne SG, Willis AC. Synthesis of furo[3,2-c]coumarins under microwave irradiation using nano-CoFe2O4@SiO2–PrNH2 as an efficient and magnetically reusable catalyst. Chemistry of Heterocyclic Compounds. 2016;52(5):288-93.
39. Dekamin MG, Eslami M, Maleki A. Potassium phthalimide-N-oxyl: a novel, efficient, and simple organocatalyst for the one-pot three-component synthesis of various 2-amino-4H-chromene derivatives in water. Tetrahedron. 2013;69(3):1074-85.
40. Safaei-Ghomi J, Enayat-Mehri N, Eshteghal F. 4-(4′-Diamino-di-phenyl)-sulfone supported on hollow magnetic mesoporous Fe 3 O 4 @SiO 2 NPs: As a reusable and efficient catalyst for the synthesis of ethyl 2-amino-5,10-dihydro-5,10-dioxo-4-phenyl-4 H benzo[g]chromene-3-carboxylates. Journal of Saudi Chemical Society. 2018;22(4):485-95.